RSC Pharmaceutics

ROYAL SOCIETY OF CHEMISTRY

PAPER

View Article Online
View Journal | View Issue

Cite this: *RSC Pharm.*, 2026, **3**, 738

In vivo translation of a dual-stimuli-responsive drug carrier based on mesoporous silica nanoparticles for the co-delivery of camptothecin and 5-fluorouracil

Debatrayee Dasgupta,[a] Sonal Thakore,*[a] Anjali Patel *[a] and Sriram Seshadri[b]

With the advent of nanotechnology, combined drug therapies employing dual-drug delivery provide an efficient way to overcome the drawbacks of conventional chemotherapy, such as lack of specificity, multi-drug resistance and low aqueous solubility. Herein, a dual-drug delivery system based on mesoporous silica nanoparticles (MSNs) was developed to target tumours with the dual-responsive co-delivery of two anticancer drugs, camptothecin (CPT) and 5-fluorouracil (5-FU), in a sequential manner. The mesopores were loaded with CPT, and subsequently, a pegylated-biotin polymer was used to coat them. The disulphide link and acid group present in the polymer contribute to the stimuli-triggered release of the drugs. Since cancer cells need biotin to continue proliferating, it functions as a targeting ligand. Mathematical modelling studies revealed that the drug-release kinetics followed a diffusion mechanism for both the hydrophobic and hydrophilic drugs. Beyond *in vitro* release and cytotoxicity assays, extensive *in vivo* biological evaluations, including liver function markers, serum biochemistry and histopathological examinations, demonstrated pronounced tumour suppression with reduced hepatic toxicity. The nanocarrier downregulated key tumour biomarkers, effectively lowered serum transaminases and restored normal liver architecture. Collectively, these findings affirm the translational potential of this smart dual-drug delivery platform for cancer therapy.

Received 20th December 2025,
Accepted 16th March 2026

DOI: 10.1039/d5pm00390c

rsc.li/RSCPharma

Introduction

Cancer is one of the most fatal diseases of recent times, and it causes millions of deaths every year. The International Agency for Research on Cancer estimates that there will be 28.4 million new instances of cancer worldwide in 2040, a 47% increase since 2020.[1–3] Conventional cancer treatments include surgery, radiation and chemotherapy.[4,5] Chemotherapy has been the backbone of traditional cancer treatment due to its great efficacy compared to other therapies. However, the clinical usage of most chemotherapeutic drugs is severely constrained since they destroy cancer cells while having lethal side effects on normal tissues due to their lack of specificity. This is one of the major reasons for failures in cancer chemotherapy and presents a significant risk to the therapeutic efficacy.[6–8]

Facing such challenges, studies on the tumour microenvironment (TME) have been performed, which demonstrated that cancer tissues exhibit a slightly more acidic environment than the normal body environment.[9] The elevated metabolic activity of cancer cells also raises local temperatures relative to those of normal tissues.[10,11] Glutathione (GSH) is a potent biological reducing tripeptide and is frequently employed as a disulfide bond (–S–S–) stimulator at certain concentrations. In response to a higher oxidative state required to maintain metabolism and malignant development, the mitochondria of cancer cells produce more GSH than those of normal tissues (ranging between 2 and 10 μmol L^{-1}).[12–14] This quantity of GSH is sufficient to break the disulfide bond. Therefore, such differences in GSH concentration could be utilised to develop smart stimuli-responsive drug carriers for controlled and targeted drug release.

A review of the literature reveals that, in recent years, intensive research has been devoted to the development of drug-delivery systems (DDSs) for targeted delivery of anticancer drugs to tumour sites and responsive release at the lesion site. Numerous internal and external stimuli-responsive approaches have been developed and explored in an attempt to accomplish appropriate drug release based on the diversity of the TME. Stimulus-responsive DDSs are classified as either internal stimuli-responsive (such as changes in pH, temperature, and

[a]*Department of Chemistry, Faculty of Science, The Maharaja Sayajirao University of Baroda, Vadodara, 390 002, India. E-mail: sonal.thakore-chem@msubaroda.ac.in, anjali.patel-chem@msubaroda.ac.in*
[b]*Institute of Science, Nirma University, Ahmedabad, 382 481, India*

enzymes) or external stimuli-responsive (such as light and magnetic fields).[15–19] However, the TME is significantly different from normal tissues, therefore, a single stimulus-responsive DDS is not sufficient to provide effective drug release. In this regard, multiple stimuli-responsive materials can better respond to the complex conditions at the lesion site and enable more controlled drug release.[20]

With the aid of nano-DDSs, in addition to the benefits of the enhanced permeability and retention (EPR) effect, specific interaction with tumour cells and stimulus-triggered drug-delivery performance in the TME can be achieved, and cancer therapy can be efficiently enhanced. Lysosomes, micelles and vesicles are among several DDSs that have been used to date. However, due to their outstanding biocompatibility, abundance of mesopores, and ease of surface modification, as well as their ability to increase the bioavailability of poorly soluble drugs, mesoporous silica nanoparticles (MSNs) continue to be the most promising material.[21] A literature survey shows some reports on MSNs being incorporated into a polymer matrix for release applications.[22–28] Despite being extensively employed to improve chemotherapy, smart DDSs with null premature release, specific cancer cell targeting and regulated release are still incapable of entirely eliminating tumour mass due to the multi-drug resistance (MDR) of tumours. To increase the effectiveness of clinical anticancer treatments, many anticancer drugs and various methods of therapy have been combined and used concurrently.[9,29–31]

Camptothecin (CPT), a naturally occurring quinoline alkaloid, is employed as an antiproliferative drug and has been studied both *in vivo* and *in vitro* against various tumours. However, due to its poor solubility in water, low plasma stability and severe toxicity, its clinical application is restricted.[32–34] CPT encapsulated in MSNs currently represents one of the most promising approaches for anticancer therapy due to its nanometer size and high specific surface area. Also, chemotherapy with 5-fluorouracil (5-FU), a fluorinated pyrimidine, is the first line of complementary therapy in cancer patients. Although 5-FU displays significant effects in cancer therapy, its non-selectivity to cancer cells, short plasma half-life (8–20 min), and toxic side effects reduce its therapeutic efficiency. Moreover, drug resistance is a very common phenomenon among cancer patients who are treated with 5-FU, so that the effectiveness of 5-FU treatment has been reported to be as low as 26%.[35–37] Therefore, nano-DDSs offer a promising solution for tackling obstacles associated with drug resistance, such as overexpression of efflux carriers of drugs and problematic apoptosis mechanisms.

Herein, a stimuli-responsive and dual-drug (both hydrophobic and hydrophilic) delivery system was developed to address the issues and challenges associated with MDR, while taking into account the TME. CPT, a hydrophobic drug, was loaded into the mesopores of MSNs. These MSNs were then encapsulated with a pegylated-biotin polymer that exhibits excellent pH and redox sensitivities. 5-FU, as a hydrophilic anti-cancer drug, was subsequently incorporated into the pegylated-biotin polymer. A growth stimulant at the cellular level, biotin (also known as vitamin H and vitamin B7) is necessary for cancer cells to maintain their high proliferative rate.[38,39] Due to the overexpression of biotin receptors on a number of cancer cells, it is utilised as a tumour-targeting agent. Vitamin H was chosen as the targeting ligand for this investigation since it is widely accepted that vitamins may target cancer cells with specificity. As a result, vitamin H becomes a powerful targeting agent that maximises the delivery of drugs to the cancer site.[40] It is notable that the proposed amphiphilic DDS has a disulphide linkage that responds to GSH concentration, resulting in a redox response, and a carboxylic acid group that is sensitive to acidic pH. Consequently, a sequential degeneration of the designed DDS is anticipated in the TME. To our knowledge, such sequentially degenerating, dual-drug and dual-stimuli responsive MSNs targeting liver cancer cell lines through biotin have not been reported to date. As shown in Scheme 1, the primary objective was to facilitate the development of a nanocarrier that features controlled and targeted drug release in response to specific stimuli by:

I. Developing a DDS that can transport a substantial dose of both hydrophilic and hydrophobic anticancer drugs by exploring the unique features of MSNs.

II. Incorporating disulphide linkages and carboxylic acid groups to enable dual-stimulus-responsive drug release triggered by elevated GSH concentration and acidic pH, respectively, enabling dual administration through combination chemotherapy.

III. Employing biotin as a targeting ligand to achieve selective delivery to cancer cells.

Experimental

Materials and methods

Cetyltriethylammoniumbromide (CTAB) was purchased from Loba Chemie Pvt. Ltd., Mumbai. Tetraethylorthosilicate (TEOS), ethanol and ammonia solution (25%) were procured

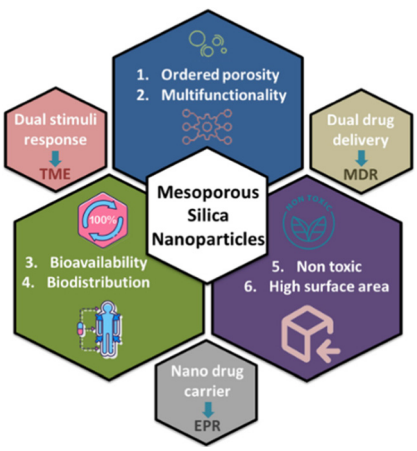

Scheme 1 Schematic of the designed multifunctional dual-drug delivery system based on MCM-48 nanoparticles.

from Merck. Solvents such as toluene, *N*,*N*-dimethylformamide (DMF), dimethylsulfoxide (DMSO), acetone and dichloromethane (DCM) were obtained from Merck. Poly(ethylene glycol) (PEG, M_n = 6.0 kg mol^{-1}), hexamethylene diisocyanate (HMDI), biotin, 1,4-diazabicyclo[2.2.2]octane (DABCO) and the drug camptothecin (CPT) were purchased from Sigma Aldrich. *N*,*N*′-Dicyclohexylcarbodiimide (DCC) and 5-fluorouracil (5-FU) were obtained from TCI chemicals, and 4-(dimethylamino)pyridine (DMAP), L-cysteine (L-cys), sodium acetate, acetic acid, and glutathione (GSH) were obtained from Sisco Research Laboratories (SRL), India. All the chemicals procured were of analytical grade and used without further purification. NIH/3T3 fibroblast and human hepatocellular liver carcinoma (HepG2) cell lines were obtained from the National Centre for Cell Science, Pune, India.

Synthesis of nMCM-48

The cubic 3-D structured nMCM-48 was synthesized using the sol–gel process in the presence of structural directing agents, following a method previously reported by our group.[41,42] In brief, 2.4 g of CTAB was dissolved in 50 mL of distilled water at 35 °C, followed by the addition of 50 mL of ethanol and 15.4 mL of 25% ammonia solution and the mixture was stirred for 15–20 min. Subsequently, 3.4 g of TEOS was added dropwise, and the mixture was stirred for an additional 2 h. The resulting white suspension was filtered, washed thoroughly with distilled water, dried at room temperature and calcined for 6 h at 550 °C. The obtained material was designated as nMCM-48.

Synthesis of dual-drug-loaded carrier

Loading of CPT into nMCM-48. The loading of CPT into nMCM-48 was carried out using the soaking method. Firstly, a solution of CPT with a concentration of 1.0 mg mL^{-1} was prepared by dissolving 20.0 mg of CPT in 20.0 mL of methanol. Subsequently, 20.0 mg of the carrier (nMCM-48) was dispersed in 20.0 mL of the 1.0 mg mL^{-1} drug solution. The solution was then sonicated for 10 min to ensure a uniform dispersion and subsequently stirred for 24 h at 37 °C to facilitate the successful loading of the drug into the pores of nMCM-48. After 24 h, the drug-loaded nanoparticles were separated by ultracentrifugation at 12 000 rpm for 15 min. The resulting solid was washed twice with acetone (5 mL) to ensure removal of any excess drug. Further, the drug-loaded nanoparticles were air-dried and placed in a desiccator for storage. The obtained material was designated as CPT/nMCM-48.

Polymer coating of CPT/nMCM-48

Step I. The PEGylated biotin polymer was synthesized *via* a DCC-mediated esterification reaction between biotin and PEG_{6000}, following a literature protocol reported previously by our group[40] as shown in Scheme 2. Briefly, biotin (0.083 mmol) and PEG_{6000} (0.083 mmol) were dissolved in DMF (10 mL) under N_2 atmosphere, followed by the addition of DCC (0.48 mmol) and DMAP (0.41 mmol) as a catalyst. The reaction mixture was stirred at room temperature for 24 h, and, after 24 h, the mixture was vacuum filtered to ensure removal of unreacted reagents and dicyclohexylurea. The product was precipitated using diethyl ether and subsequently collected by vacuum filtration. The product was vacuum dried, stored in a desiccator and designated as PEGylated biotin polymer.

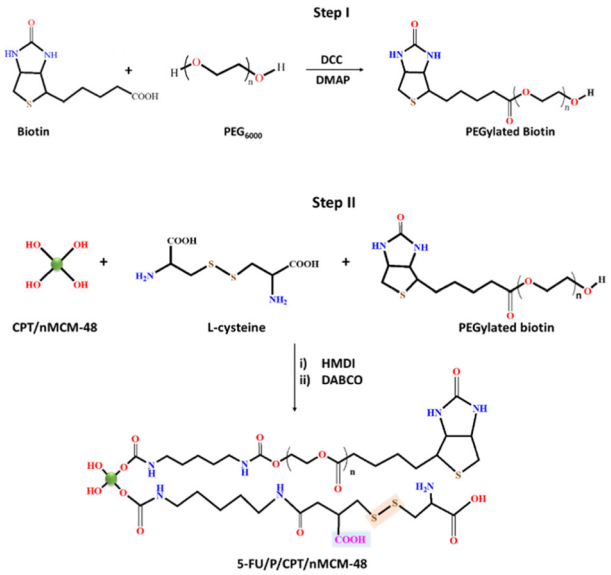

Scheme 2 Schematic of the surface functionalization of CPT-loaded nMCM-48 with a dual-responsive polymer.

Step II. To functionalize the surface of CPT/nMCM-48 with the biocompatible stimuli-responsive polymer, 50.0 mg of CPT/nMCM-48 was taken in a round-bottom flask, and 5.0 mL of anhydrous DMF was added. The mixture was stirred for 5 min, followed by the addition of L-cys, a bifunctional disulfide-containing amino acid to introduce redox-sensitive disulfide bonds. After 30 min of stirring, the previously synthesized PEGylated biotin polymer (50.0 mg) was added to impart tumour-targeting ability through biotin receptor interactions. Throughout the process, an inert N_2 atmosphere was maintained to prevent oxidative degradation of thiol groups. While the inert N_2 ambient condition was sustained, the reaction mixture was supplemented with 250.0 μL of HMDI to induce cross-linking and 3.5 mg of DABCO as a bifunctional isocyanate linker as well as catalyst. After 24 h, the reaction mass was transferred to distilled water to facilitate precipitation. The resulting polymer-functionalized nanoparticles were then filtered and air-dried for another 24 h. The obtained dual-functional material was designated as P/CPT/nMCM-48 (Scheme 2).

Loading of 5-FU. The process of loading 5-FU was carried out using the same soaking technique employed for loading CPT. Briefly, 20.0 mg of the carrier, P/CPT/nMCM-48 was suspended in 20.0 mL of 1.0 mg mL^{-1} drug solution of 5-FU in water. This solution was sonicated for 10 min and further stirred for 24 h at 37 °C. The solid was then separated by ultracentrifugation and washed with ethanol twice. The drug-loaded material was then air-dried and stored in a desiccator.

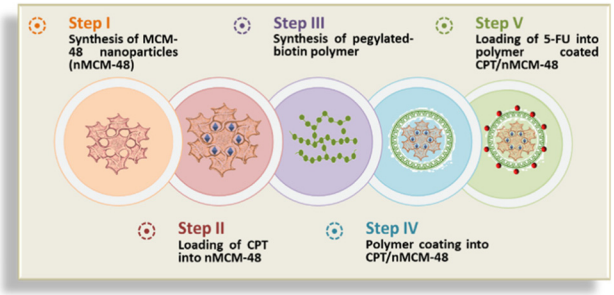

Scheme 3 Schematic of the stepwise synthesis of the designed dual-drug delivery system showing dual stimuli-responses.

The obtained material was designated as 5-FU/P/CPT/nMCM-48 (Scheme 3).

In order to determine the concentration of free drug in the supernatant, calibration curves for CPT and 5-FU were plotted using their absorptions at 225 nm and 266 nm, respectively. The amount of drug entrapment was then calculated using the absorbance obtained for the supernatant. Therefore, the % entrapment efficiency of both drugs, CPT and 5-FU, was calculated by using the following equation:

$$\%\text{Entrapment efficiency} = \frac{D_i - D_f}{D_i} \times 100$$

where, D_i denotes the initial concentration of both the drugs taken, while D_f denotes the concentration of both the drugs in the supernatant. Furthermore, the %drug loading content of both the drugs was calculated using the following formula:

$$\%\,\text{Drug loading} = \frac{\text{Amount of drug loaded}}{\text{Amount of carrier used}} \times 100.$$

Stimuli-responsive drug release

In a typical drug-release experiment, 5.0 mg of the drug-loaded nanoparticles were suspended in 10.0 mL of release medium, SGF, with 1 mM, 10 mM and without GSH, at 37 °C under stirring. At predetermined intervals, 3.0 mL of the incubation medium was withdrawn for analysis and replaced with the same volume of fresh buffer. By using a UV-Visible spectrophotometer (PerkinElmer Lambda 35) at a wavelength of 225 nm for CPT and 266 nm for 5-FU, the extracted medium was evaluated.

Physicochemical characterizations

A HR-TEM (model-JEM 2100) operating at an accelerating voltage of 200 kV was used to study the morphology of the synthesised nanoparticles. Samples were prepared by dispersing the nanoparticles in ethanol, followed by ultrasonication, and a drop of the suspension was placed onto a carbon-coated copper grid and dried under ambient conditions prior to imaging. Using pellets of potassium bromide (KBr), the FT-IR was analysed with a Shimadzu (IRAffinity-1S) instrument in the range of 4000–400 cm^{-1} with a spectral resolution of 4 cm^{-1}, and each spectrum was obtained by averaging 32 scans. DLS was used to estimate the distribution of particle sizes and their average diameter in deionized water; the analysis was performed with a Beckman Coulter Delso Nano. A Zetasizer Nano ZSP (ZEN 5600) was used to measure the Z-potential of the nanoparticles. Using a thermal gravimetric analyzer (Mettler Toledo Star SW 7.01) under a nitrogen atmosphere in the temperature range of 30–600 °C, with a flow rate of 2 mL min^{-1} and a heating rate of 10 °C min^{-1}, the stability of the nanoparticles was observed at higher temperatures. All the characterizations related to nMCM-48 and pegylated-biotin were previously reported by our group.[40,42] The same are incorporated here for better comparison and for the convenience of the readers.

In vitro cellular uptake determined by the MTT assay

The cytocompatibility and anticancer efficacy of the synthesized nanocarriers were evaluated using the MTT [3-(4,5-dimethylthiazol-2-yl)-2,5-diphenyltetrazolium bromide] colorimetric assay. NIH/3T3 fibroblast cells and HepG2 hepatocellular carcinoma cells were cultured in Dulbecco's Modified Eagle Medium (DMEM) supplemented with 10% fetal bovine serum (FBS) and 1% penicillin streptomycin, maintained at 37 °C in a humidified incubator with 5% CO_2. For the assay, cells were seeded at a density of 5×10^4 cells per well in a 96-well plate and allowed to adhere for 24 h. To assess biocompatibility, NIH/3T3 cells were incubated with unloaded nanocarriers at increasing concentrations (0–250 μg mL^{-1}). For cytotoxicity analysis, HepG2 cells were treated with CPT, 5-FU, P/CPT/nMCM-48 and 5-FU/P/CPT/nMCM-48 at equivalent total drug concentrations. Following 24 h of exposure, MTT solution was added to each well. The resulting formazan crystals were dissolved in dimethyl sulfoxide (DMSO), and the absorbance was measured at 570 nm using a microplate reader (Synergy HTX Bio-Tek Instruments, Inc., Winooski, VT). All experiments were conducted in triplicate, and the cell viability was expressed as a percentage relative to untreated controls using the following equation:

$$\text{Vaibility} = \frac{\text{Absorbance of the cells treated with test compound}}{\text{Absorbance of the untreated control cells}} \times 100.$$

In vivo antitumor efficacy

All animal studies were conducted in accordance with the guidelines of the Committee for the Purpose of Control and Supervision of Experiments on Animals (CPCSEA), India, and were approved by the Institutional Animal Ethics Committee. Both male and female Balbc mice (28–30 g) were used for the evaluation of *in vivo* antitumor activity. Hepatocellular carcinoma was induced by injecting 1×10^6 HepG2 cells intraperitoneally. Animals were randomly divided into five groups: control, untreated, 5-FU treated, CPT treated and 5-FU/P/CPT/nMCM-48 treated. The treatments were administered intravenously for 14 consecutive days. At the end of the study, body and liver weights were recorded. Blood samples were collected *via* puncturing of the retro-orbital sinus, and serum was separ-

ated with a cold centrifuge at 3000 rpm for biochemical analysis. Levels of serum glutamic oxaloacetic transaminase (SGOT), serum glutamic pyruvic transaminase (SGPT), total cholesterol, triglycerides, high-density lipoprotein (HDL), and low-density lipoprotein (LDL) were measured using commercially available diagnostic kits (Reckon Diagnostics Ltd, Vadodara, India). Liver tissues were harvested and stained with hematoxylin and eosin (H&E) for histopathological evaluation under light microscopy (40× and 100× magnification). Tissue architecture, including hepatocyte integrity, necrosis, sinusoidal dilation and the presence of dysplastic nodules, was assessed. Additionally, the expression of liver tumour biomarkers, including matrix metalloproteinase-2 (MMP-2), MMP-9 and alpha-fetoprotein (AFP), was quantified using enzyme-linked immunosorbent assay (ELISA) kits (Krishgen Biosystems, Mumbai, India). After termination of the experiments, animals were sacrificed under mild ether anaesthesia, and a liver autopsy was conducted.

Physicochemical characterizations

HR-TEM images of the synthesized nanoparticles are shown in Fig. 1. The morphology of the nanoparticles shows that the nanocarriers are spherical in shape with uniform size and good dispersion. After loading CPT into the mesopores of nMCM-48, the spherical morphology of the MSNs does not change. Further, after modification with pegylated-biotin polymer and subsequent 5-FU loading, the spherical shape remains unaltered. From the micrographs, it is evident that, after modification in each step (Fig. 1b–e), the spheres of nMCM-48 appear to be darker compared to the original (Fig. 1a), indicating successful drug loading and polymer coating.

The hydrodynamic diameter, zeta potential and polydispersity by the number weighted distribution were determined using DLS. DLS confirmed the apparently monodisperse distribution of particle sizes, showing a narrow hydrodynamic size distribution around 141 ± 2.6 nm for CPT/nMCM-48 (Fig. 2). Coating the nanocarrier with stimuli-responsive polymer

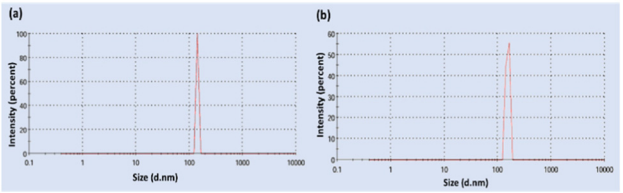

Fig. 2 Average hydrodynamic size of (a) CPT/nMCM-48 and (b) 5-FU/P/CPT/nMCM-48.

(5-FU/P/CPT/nMCM-48) resulted in an increase in hydrodynamic size distribution to 154 ± 3.1 nm. A slight increase in the hydrodynamic radius was observed in the latter case, indicating the successful polymer coating. The nanoparticles have an average size of approximately 150 nm; notably, due to the EPR effect, nanoparticles smaller than 200 nm can be better enriched at the tumour site. The polydispersity index (PDI) for the polymer-coated formulation, 5-FU/P/CPT/nMCM-48, was found to be 0.042, a value indicative of a highly uniform size distribution and excellent dispersibility.

The zeta potential values of CPT/nMCM-48 and 5-FU/P/CPT/nMCM-48 are −1.86 ± 0.18 mV and −3.02 mV ± 0.22 mV, respectively. These values indicate that the nanoparticles remain negatively charged after surface coating, and the structure of nMCM-48 remains unchanged. It is considered that nanoparticles can maintain high colloidal stability when the zeta potential is less than −30 mV. As the particle disulfide concentration increases, the zeta potential becomes more negative, which aligns with previous findings, possibly due to variations in surface silanol density (Fig. 3).

FT-IR spectroscopy was employed to examine the structural characteristics of nMCM-48 and its sequentially modified formulations (Fig. 4). The spectrum of nMCM-48 exhibited characteristic Si–O–Si asymmetric stretching vibrations in the 1100–1250 cm^{-1} region, along with symmetric stretching at 578 cm^{-1} and Si–O bending at 462 cm^{-1}, confirming preservation of the mesoporous silica framework. Pure CPT displayed prominent carbonyl stretching bands at 1743 and 1652 cm^{-1} together with aromatic vibrations around 1442 and 771 cm^{-1}. After CPT incorporation, the presence of these carbonyl and aromatic bands alongside the silica framework signals indicated successful drug accommodation within the mesoporous structure. Subsequent polymer functionalization introduced additional spectral features associated with ester groups (C═O

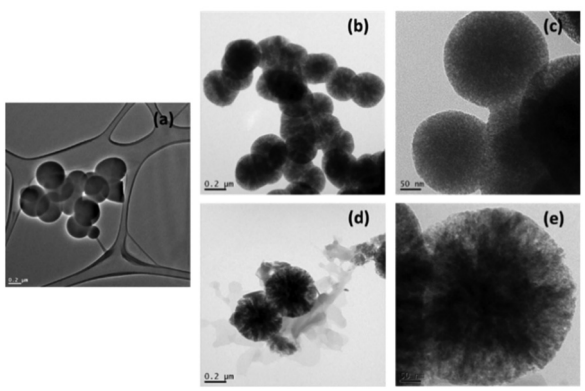

Fig. 1 HR-TEM micrographs of (a) nMCM-48; (b and c) CPT/nMCM-48; and (d and e) 5-FU/P/CPT/nMCM-48.

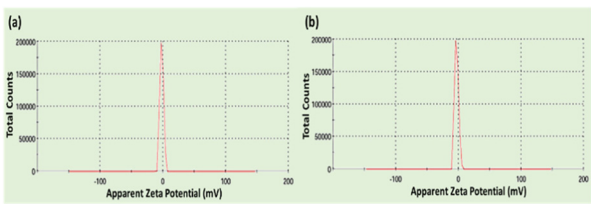

Fig. 3 Zeta potential values of (a) CPT/nMCM-48 and (b) 5-FU/P/CPT/nMCM-48.

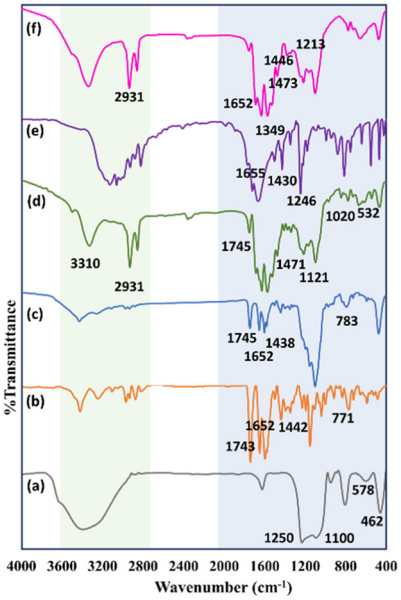

Fig. 4 FT-IR spectra of (a) nMCM-48, (b) CPT, (c) CPT/nMCM-48 (d) P/CPT/nMCM-48, (e) 5-FU and (f) 5-FU/P/CPT/nMCM-48.

and C–O) as well as PEG-related –OH stretching vibrations. Bands observed near 2931 cm^{-1} (aliphatic C–H stretching), 1471 cm^{-1} (C–H bending) and 1020 cm^{-1} (C–N stretching) are consistent with functional groups present in the biotin moiety, supporting the presence of the biotin-functionalized polymer coating. The spectrum of pure 5-FU exhibited characteristic peaks corresponding to C═O stretching (1652 cm^{-1}), C–F vibration (1473 cm^{-1}), C–N stretching (1213 cm^{-1}) and pyrimidine ring vibration (1368 cm^{-1}). For 5-FU/P/CPT/nMCM-48, spectral features attributable to silica, CPT, polymer, biotin and 5-FU were simultaneously observed, indicating successful dual-drug incorporation while maintaining the structural integrity of the carrier. Although partial band overlap is expected in such multicomponent systems, the sequential spectral changes observed after each modification step collectively support the intended structural assembly.

TGA measured an overall weight loss of 10.8% for nMCM-48 and 88.7% for 5-FU/P/CPT/nMCM-48 after heating to 500 °C (Fig. 5). The TGA curves show a gradual decline in loss from nMCM-48 to 5-FU/P/CPT/nMCM-48. The higher % loss observed in the case of P/CPT/nMCM-48 and 5-FU/P/CPT/nMCM-48 may be attributed to the degradation of both the drug molecules and the polymer coating. This indicates the successful loading of both the drugs and the polymer coating onto the surface of the MSNs.

In vitro release study

The extensive application of MSNs in the biomedical and pharmaceutical fields is due to their ability to accommodate both hydrophobic and hydrophilic molecules within their pores. Model drugs CPT and 5-FU were both utilized in the study. Methanol was chosen as the solvent to achieve drug loading of the hydrophobic CPT onto MSN using the soaking

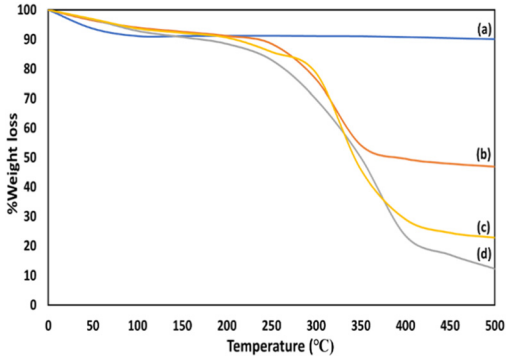

Fig. 5 TGA curves of (a) nMCM-48 (b) CPT/nMCM-48 (c) P/CPT/nMCM-48 and (d) 5-FU/P/CPT/nMCM-48.

method. After 24 h, analysis of the supernatant showed an entrapment efficiency of 71.8% for CPT, corresponding to a final loading of 14.4 wt% (0.144 mg CPT per mg of carrier). Conversely, the hydrophilic drug 5-FU was loaded using water as the appropriate solvent, resulting in an entrapment efficiency of 85.8%, corresponding to a loading of 17.2 wt% (0.172 mg 5-FU per mg of carrier).

As discussed in the introduction, the TME is generally characterized by a slightly acidic pH and elevated intracellular GSH concentration compared to normal tissues. Therefore, in order to better simulate the physiological tumour environment, the *in vitro* drug release behaviour of the nanocarrier was evaluated at pH 5.0 in the absence of GSH and in the presence of different GSH concentrations (1 mM and 10 mM) for a period of 10 h (Fig. 6). In the absence of GSH, both drugs

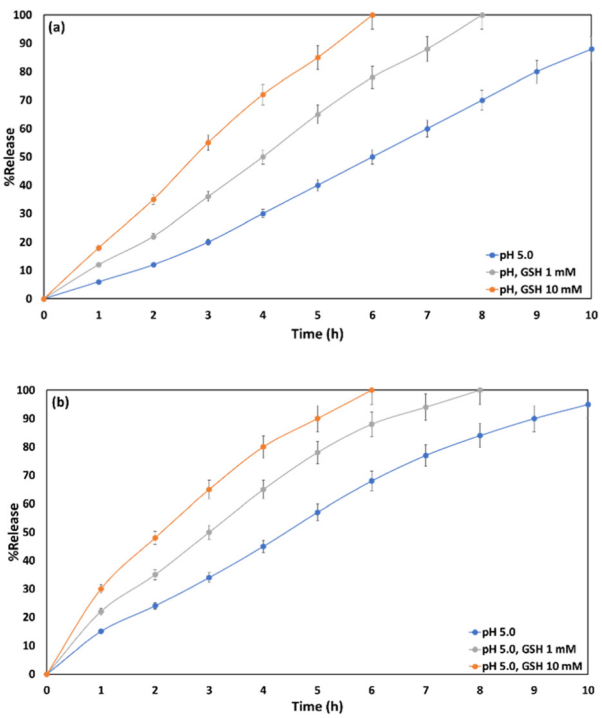

Fig. 6 *In vitro* release under different redox conditions for (a) CPT and (b) 5-FU from 5-FU/P/CPT/nMCM-48.

exhibited a slower and sustained release behaviour, with 88.0% of CPT and 95.0% of 5-FU released after 10 h, indicating that the nanocarrier maintains structural stability at pH 5.0. Further, 5-FU exhibited faster release due to its smaller molecular size, higher hydrophilicity and weaker interactions with the mesoporous silica framework. In contrast, CPT demonstrated a more sustained release profile owing to its relatively hydrophobic nature and stronger interactions with the pore surface, resulting in greater confinement within the carrier matrix. Upon addition of 1 mM GSH, the release of both drugs increased significantly, reaching 99.9% for CPT and 99.8% for 5-FU within 8 h, demonstrating the redox-responsive nature of the system. When the GSH concentration was further increased to 10 mM, a more rapid release behaviour was observed, with almost complete release of CPT (99.8%) and 5-FU (99.9%) occurring within 6 h.

The comparative release data under different redox conditions are summarized in Table 1. It can be clearly observed that drug release increases with increasing GSH concentration, confirming the GSH-responsive behaviour of the system. This phenomenon can be attributed to the reductive cleavage of disulfide (–S–S–) linkages present in the nanocarrier architecture. At higher GSH concentrations, these linkages undergo sequential reduction, resulting in structural destabilization and facilitating the release of the encapsulated drugs.

Overall, the release study demonstrates that the designed nanocarrier exhibits dual responsiveness toward pH 5.0 and reductive GSH environments, which are key characteristics of the tumour microenvironment, thereby highlighting its potential for stimuli-responsive and targeted drug delivery in cancer therapy.

Table 1 %Release of CPT and 5-FU at different conditions

		%Release (at the end of 10 h)		
			With GSH	
pH	Drug	Without GSH	GSH 1 mM	GSH 10 mM
5.0	CPT	88.0	99.9 (8 h)	99.8 (6 h)
	5-FU	95.0	99.8 (8 h)	99.9 (6 h)

Release kinetics and mechanism

Since enhanced drug release was obtained at pH 5.0 with 10 mM GSH, these optimized conditions were chosen for further evaluation of the drug release kinetics and mechanism. The cumulative release profiles of CPT and 5-FU were analysed by fitting the data into standard kinetic models, including zero-order, first-order and Higuchi models, to understand the underlying mechanism of drug release from the nanocarrier, as shown in Table 2. The calculated correlation coefficients (R^2) indicated that CPT exhibited the best fit with the zero-order model (R^2 = 0.9965), suggesting nearly constant and controlled release behaviour over time. In contrast, 5-FU showed the highest linearity with the Higuchi model (R^2 = 0.9838), indicating that its release was predominantly governed by diffusion from the carrier matrix. This difference in release behaviour can be attributed to the distinct loading locations of the two drugs within the nanocarrier architecture. CPT, which is primarily confined within the mesoporous silica framework, undergoes more controlled release as the matrix effectively regulates the release of CPT, allowing sustained and controlled drug delivery. Conversely, 5-FU, which is incorporated after polymer coating, diffuses through the polymeric layer, resulting in a diffusion-controlled release profile consistent with the Higuchi model. The lower R^2 values obtained for the remaining kinetic models further confirm that the release process is not purely governed by concentration-dependent kinetics but is largely regulated by matrix diffusion and the structural architecture of the nanocarrier system.

In vitro cytotoxicity – MTT assay

To evaluate the cytocompatibility of the synthesized polymer-conjugated silica nanocarrier, 5-FU/P/CPT/nMCM-48, an MTT colorimetric assay was performed using the NIH/3T3 fibroblast cell line as a model for normal mammalian cells. Cells were incubated with increasing concentrations of the unloaded nanocarriers (up to 250 μg mL^{-1}) for 24 h. The obtained results show that the nanocarriers demonstrated minimal cytotoxic effects, maintaining a cell viability of >80% over the concentration range tested, confirming their excellent biocompatibility and potential suitability for drug-delivery applications.

To assess antineoplastic efficacy, the HepG2 human hepatocellular carcinoma cell line was employed. The nanocarriers were loaded with CPT, 5-FU, as well as the nano formulation

Table 2 Mathematical models of drug-release kinetics with correlation coefficient values

		Value of corresponding kinetic constants		Value of correlation coefficient (R^2)	
Models	Equation	CPT	5-FU	CPT	5-FU
Zero-order	$C_t = C_0 + K_0 t$	16.82	16.14	0.9965	0.9649
First-order	$\log C_t = \log C_0 - K_1 t/2.303$	0.374	0.448	0.9547	0.9729
Higuchi	$C_t = K_H \times t^{1/2}$	41.75	41.89	0.9293	0.9838

Here, C_t represents the quantity of drug released at time t, while C_0 corresponds to the initial amount of drug present in the medium (generally taken as zero). The constants K_0, K_1 and K_H denote the release rate constants for zero-order, first-order and Higuchi models, respectively.

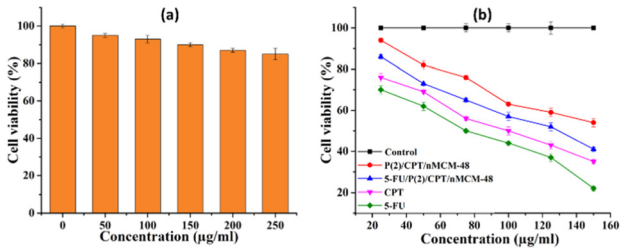

Fig. 7 *In vitro* cytotoxicity and anticancer activity of the formulations, (a) NIH/3T3 fibroblast cells treated with 5-FU/P/CPT/nMCM-48 (up to 250 μg mL^{-1}) for 24 h, assessed by the MTT assay, and (b) HepG2 cells treated with CPT, 5-FU, CPT/nMCM-48, and 5-FU/P/CPT/nMCM-48 at equivalent concentrations (up to 150 μg mL^{-1}) for 24 h. Results are expressed as mean ± SD (n = 3), with statistical significance set at p < 0.05.

(5-FU/P/CPT/nMCM-48) and administered at equivalent total drug concentrations (Fig. 7). The drug-loaded formulations demonstrated moderate cytotoxicity, with CPT-loaded carriers reducing cell viability up to 54% at 150 μg mL^{-1}. Notably, the designed dual-drug-loaded formulation further enhanced the cytotoxic effects, reducing viability to 41% under identical conditions. The pronounced reduction in cellular viability upon combinatorial treatment suggests a synergistic cytotoxic interaction, likely attributable to complementary mechanisms of action of CPT, being a topoisomerase I inhibitor, and 5-FU, acting as an antimetabolite *via* thymidylate synthase inhibition. These findings underscore the potential of the designed dual-drug delivery system to enhance therapeutic efficacy through simultaneous modulation of multiple cancer cell survival pathways.

In vivo antitumor efficacy of the dual-responsive nanocarrier

To validate the translational potential of the dual-drug delivery nanoplatform, the *in vivo* antitumor efficacy of the synthesized nanocarriers was assessed using the liver-cancer-induced Balbc mouse model. Treatment groups included animals administered with free CPT, free 5-FU, and the dual-drug-loaded system 5-FU/P/CPT/nMCM-48. After 14 days of intravenous administration, body weight and liver weight were monitored as general indicators of systemic toxicity and organ burden.

Body metrics and tumour-associated biomarkers

As shown in Fig. 8a and b, no significant weight loss was observed in the treatment groups compared to the control, indicating the biocompatibility and systemic safety of the nanocarriers. Notably, the group treated with 5-FU/P/CPT/nMCM-48 demonstrated a statistically significant reduction in liver weight (p < 0.01) compared to both the free-drug-treated and untreated groups, reflecting the effective suppression of hepatic tumour proliferation.

To elucidate the molecular landscape underlying the observed phenotypic changes, tumour-specific biomarkers were analysed. The obtained results demonstrated significantly

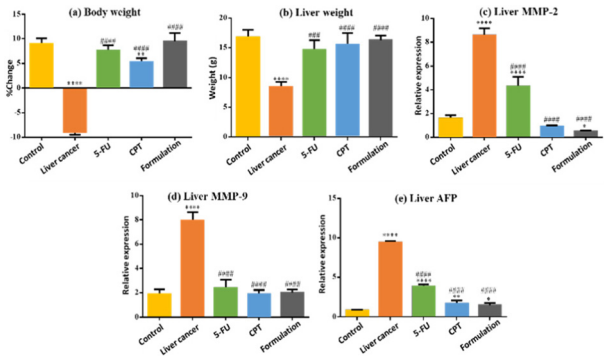

Fig. 8 Assessment of (a) body weight, (b) liver weight, along with comparison of markers of tumour progression (c) MMP-2, (d) MMP-9 and (e) AFP in mice across different treatment groups (presented as mean ± SD, n = 4). Statistical significance is denoted in the figures as * for comparisons with the control group and # for comparisons with the liver-cancer-induced group. Significance thresholds are as follows: *p < 0.05, ** or ##p < 0.01, ***p < 0.001 and **** or ####p < 0.0001.

decreased levels of key liver tumour markers, AFP, MMP-2 and MMP-9 in mice treated with the dual-drug nanocarrier, compared to all other treatment groups (p < 0.001) (Fig. 8c–e). These biomarkers are critical indicators of tumour aggressiveness and metastatic potential. The suppression of matrix metalloproteinases (MMPs) indicates reduced metastatic potential, while decreased AFP levels corroborate effective tumour inhibition. These findings reinforce the notion that the stimuli-responsive DDS enabled localized and sustained release of therapeutic agents within the tumour microenvironment, resulting in efficient tumour regression.

Histopathological evaluation

Haematoxylin and eosin (H&E) stained liver sections revealed extensive dysplastic changes, sinusoidal dilation and disrupted hepatocyte architecture in untreated tumour-bearing animals. In contrast, liver tissues from animals treated with 5-FU/P/CPT/nMCM-48 maintained normal lobular structure with minimal necrosis and preserved hepatocyte morphology (Fig. 9

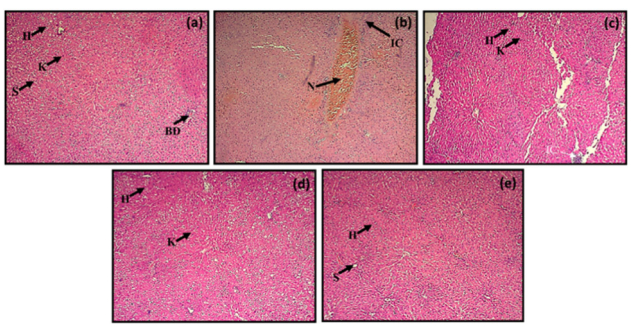

Fig. 9 Histological examination of the liver in the (a) negative control, (b) positive control and treatment groups: (c) 5 FU, (d) CPT and (e) 5-FU/P/CPT/nMCM-48 at 40× magnification. Arrows indicate H-hepatocytes, K-Kupffer cells, BD-bile duct, S-sinusoidal spaces, N-necrosis, and IC-immune cells.

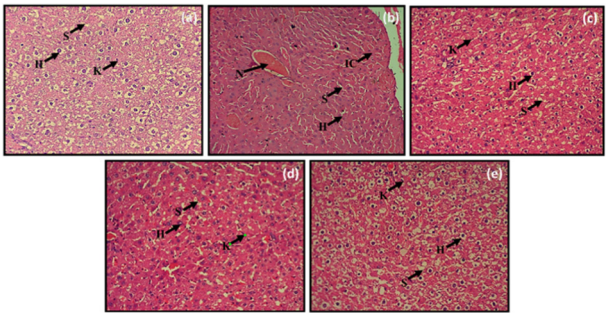

Fig. 10 Histological examination of the liver in the (a) negative control, (b) positive control and treatment groups: (c) 5 FU, (d) CPT and (e) 5-FU/P/CPT/nMCM-48 at 100× magnification. Arrows indicate H-hepatocytes, K-Kupffer cells, BD-bile duct, S-sinusoidal spaces, N-necrosis, and IC-immune cells.

and 10). These findings clearly demonstrate the therapeutic potential of the nanocarrier in restoring normal hepatic architecture following the dual-drug treatment.

Serum biochemistry

Biochemical analyses of the hepatotoxic biomarkers, SGOT and SGPT, indicated substantial elevation in the untreated group, pointing to hepatic damage induced by tumour progression. The 5-FU/P/CPT/nMCM-48 treated group exhibited the most pronounced reduction in SGOT and SGPT levels among all groups, supporting the hepatoprotective effect of the nanocarrier system and efficient tumour regression (Fig. 11). In contrast, the levels of these transaminases in the 5-FU/P/CPT/nMCM-48-treated group were significantly attenuated, approaching near-normal values, thereby demonstrating hepatoprotective effects of the DDS through tumour regression. Furthermore, lipid profile assessments revealed restoration of HDL levels and significant reductions in LDL and triglycerides in the treated cohort, correlating with improved systemic health.

The observed enhanced therapeutic outcomes can be attributed to the hierarchical disassembly mechanism of the nanocarrier triggered by the TME. The acid-responsive carboxylic acid groups enabled the early-stage release of 5-FU in the extracellular acidic milieu, while the intracellular GSH-triggered disulfide bond cleavage resulted in the sequential release of CPT inside tumour cells. This temporal and spatially coordinated release likely contributed to the synergistic therapeutic effect. In addition, the use of biotin as a targeting moiety leveraged receptor-mediated endocytosis in HepG2 cells, enhancing tumour-specific accumulation and internalization. Altogether, the *in vivo* experiments affirm that the dual-drug-loaded, dual-responsive nanocarrier not only enhances the anticancer efficacy of CPT and 5-FU but also minimizes off-target toxicity. The combination strategy employing sequential, stimuli-triggered drug release and active targeting through biotin demonstrates a promising route for addressing multidrug resistance and improving therapeutic outcomes in liver cancer.

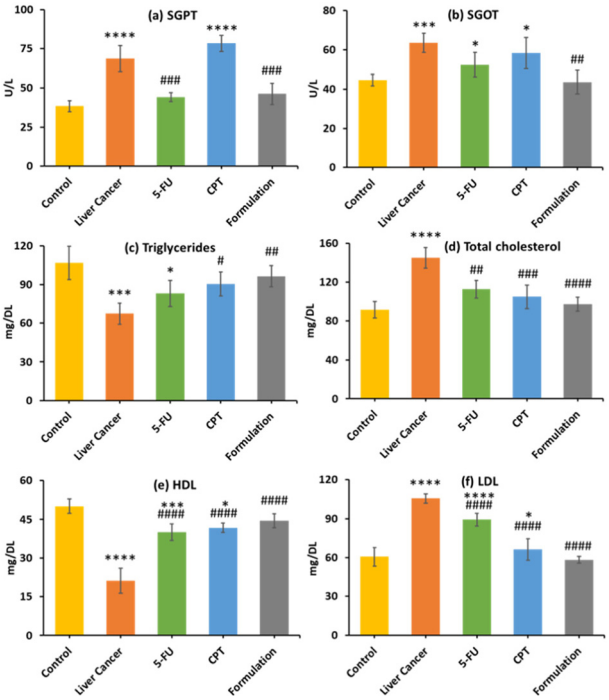

Fig. 11 Evaluation of (a) SGPT, (b) SGOT, (c) triglycerides, (d) total cholesterol, (e) HDL and (f) LDL levels across different treatment groups (expressed as mean ± SD, n = 4). Statistical significance is indicated in the figure as * for comparisons with the control group and # for comparisons with the liver-cancer-induced group. Levels of significance: *p < 0.05, ** or ##p < 0.01, ***p < 0.001, **** or ####p < 0.0001.

Conclusions

To summarise, a dual-stimuli-responsive MSN-based drug carrier was developed for the targeted co-delivery of CPT and 5-FU. Functionalized with PEGylated biotin as well as engineered with disulfide and carboxylic acid groups, the carrier enabled stimuli-triggered sequential drug release. Biotin-targeting facilitated selective uptake by HepG2 liver cancer cells. Release kinetics demonstrated that drug release followed the Higuchi model, confirming a predominantly diffusion-controlled mechanism for both CPT and 5-FU. *In vitro* assays confirmed the synergistic cytotoxicity of the formulation, while *in vivo* evaluations highlighted its clinical promise. Specifically, treatment with 5-FU/P/CPT/nMCM-48 resulted in significant tumour regression accompanied by downregulation of AFP, MMP-2 and MMP-9, restoration of normal liver histoarchitecture, as well as normalization of serum transaminases along with lipid profile. These comprehensive biological outcomes underscore the ability of the designed system not only to enhance anticancer efficacy but also to mitigate systemic toxicity. Altogether, this multifunctional nanoplatform offers a promising strategy for overcoming multidrug resistance and improving therapeutic outcomes through the integration of active targeting, dual-stimuli responsiveness and synergistic chemotherapy.

Author contributions

Debatrayee Dasgupta: conceptualization, investigation, formal analysis, writing – original draft. Sonal Thakore: conceptualization, methodology, writing – review & editing. Anjali Patel: conceptualization, supervision. Sriram Seshadri: data curation, investigation.

Conflicts of interest

There are no conflicts to declare.

Data availability

Data are available from the corresponding author upon reasonable request.

Acknowledgements

All the authors acknowledge the Department of Chemistry, The Maharaja Sayajirao University of Baroda, for thermal analysis. ST is grateful to the DST-SERB Power Grant (SPG/2021/0003149), New Delhi, India, for financial assistance. DD is thankful to SHODH (Scheme of Developing High Quality Research, KCG/SHODH/2022-23/) for providing financial support.

References

1 M. C. Velho, V. L. Winck, C. d. S. Mariot, J. N. Scholl, A. F. Weber, R. d. K. Souza, F. Visioli, F. Figueiró, M. Deon, D. A. Pilger and R. C. R. Beck, *ACS Biomater. Sci. Eng.*, 2025, **11**, 4231–4244.
2 N. U. Khaliq, J. Lee, J. Kim, Y. Kim, S. Yu, J. Kim, S. Kim, D. Sung and H. Kim, *MDPI*, 2023, preprint, DOI: 10.3390/pharmaceutics15051432.
3 Z. Wang, Y. Jiang, H. Shang, N. Qiao, X. Sun, Q. Li, X. Wang, Y. Wu and H. Ma, *J. Polym. Res.*, 2023, **30**, 210.
4 M. Arruebo, N. Vilaboa, B. Sáez-Gutierrez, J. Lambea, A. Tres, M. Valladares and Á. González-Fernández, *Cancers*, 2011, **3**, 3279–3330.
5 G. N. Hortobagyi, F. C. Ames, A. U. Buzdar, S. W. Kau, M. D. McNeese, D. Paulus, V. Hug, F. A. Holmes, M. M. Romsdahl, G. Fraschini, C. M. McBride, R. G. Martin and E. Montague, *Cancer*, 1988, **62**, 2507–2516.
6 D. B. Abreu and J. R. Cernadas, *Curr. Opin. Allergy Clin. Immunol.*, 2022, **22**, 221–225.
7 Z. Jing, Q. Du, X. Zhang and Y. Zhang, *Chem. Eng. J.*, 2022, **446**, 137147.
8 S. Ramezanian, J. Moghaddas, H. Roghani-Mamaqani and A. Rezamand, *Sci. Rep.*, 2023, **13**, 20194.
9 K. Gou, W. Xin, J. Lv, Z. Ma, J. Yang, L. Zhao, Y. Cheng, X. Chen, R. Zeng and H. Li, *Colloids Surf., B*, 2023, **221**, 113027.
10 S. Mura, J. Nicolas and P. Couvreur, *Nat. Mater.*, 2013, **12**, 991–1003.
11 Y. Qiao, J. Wan, L. Zhou, W. Ma, Y. Yang, W. Luo, Z. Yu and H. Wang, *WIREs Nanomed. Nanobiotechnol.*, 2018, **11**(1), e1527.
12 M. Mozafarinia, S. Karimi, M. Farrokhnia and J. Esfandiari, *Microporous Mesoporous Mater.*, 2021, **3316**, 110950.
13 M. Cheng, Y. Yu, W. Huang, M. Fang, Y. Chen, C. Wang, W. Cai, S. Zhang, W. Wang and W. Yan, *ACS Biomater. Sci. Eng.*, 2020, **6**, 4985–4992.
14 X. Zhang, M. Chen, Y. Kan, Y. Dong, X. Zhang, X. Wang, H. Su, S. Xu and X. Yan, *J. Mater. Sci.*, 2023, **58**, 2764–2781.
15 P. Mi, *Theranostics*, 2020, **10**, 4557–4588.
16 J. Zhou, M. Wang, H. Ying, D. Su, H. Zhang, G. Lu and J. Chen, *ACS Biomater. Sci. Eng.*, 2018, **4**, 2404–2411.
17 B. Qian, Q. Zhao and X. Ye, *J. Cardiovasc. Pharmacol.*, 2020, **76**, 414–426.
18 S. Nastyshyn, Y. Stetsyshyn, J. Raczkowska, Y. Nastishin, Y. Melnyk, Y. Panchenko and A. Budkowski, *MDPI*, 2022, preprint, DOI: 10.3390/polym14194245.
19 Y. Stetsyshyn, J. Raczkowska, K. Harhay, K. Gajos, Y. Melnyk, P. Dąbczyński, T. Shevtsova and A. Budkowski, *Colloid Polym. Sci.*, 2021, **299**, 363–383.
20 K. Thirupathi, M. Santhamoorthy, S. Radhakrishnan, S. Ulagesan, T.-J. Nam, T. T. V. Phan and S.-C. Kim, *Pharmaceutics*, 2023, **15**, 795.
21 J. Shen, Q. He, Y. Gao, J. Shi and Y. Li, *Nanoscale*, 2011, **3**, 4314.
22 M. Stanzione, N. Gargiulo, D. Caputo, B. Liguori, P. Cerruti, E. Amendola, M. Lavorgna and G. G. Buonocore, *Eur. Polym. J.*, 2017, **89**, 88–100.
23 Y. Kamachi, B. P. Bastakoti, S. M. Alshehri, N. Miyamoto, T. Nakato and Y. Yamauchi, *Mater. Lett.*, 2016, **168**, 176–179.
24 C. P. Silveira, L. M. Apolinário, W. J. Fávaro, A. J. Paula and N. Durán, *ACS Biomater. Sci. Eng.*, 2016, **2**, 1190–1199.
25 M. Zhu, Y. Zhu, L. Zhang and J. Shi, *Sci. Technol. Adv. Mater.*, 2013, **14**(4), 045005.
26 E. Zúñiga, L. Belmar, L. Toledo, C. Torres, B. L. Rivas, S. A. Sánchez and B. F. Urbano, *Eur. Polym. J.*, 2017, **95**, 358–367.
27 P. Zhao, H. Liu, H. Deng, L. Xiao, C. Qin, Y. Du and X. Shi, *Colloids Surf., B*, 2014, **123**, 657–663.
28 Y. Hu, X. Dong, L. Ke, S. Zhang, D. Zhao, H. Chen and X. Xiao, *J. Mater. Sci.*, 2017, **52**, 3095–3109.
29 Z. Omran, P. Scaife, S. Stewart and C. Rauch, *Semin Cancer Biol.*, 2017, **43**, 42–48.
30 I. S. Mohammad, W. He and L. Yin, *Crit. Rev. Ther. Drug Carrier Syst.*, 2020, **37**, 473–509.
31 Y. Liu, M. Zhu, M. Meng, Q. Wang, Y. Wang, Y. Lei, Y. Zhang, L. Weng and X. Chen, *Chin. Chem. Lett.*, 2013, **34**(1), 107583.

32 M. Berrada, A. Serreqi, F. Dabbarh, A. Owusu, A. Gupta and S. Lehnert, *Biomaterials*, 2005, **26**, 2115–2120.
33 N. Khaiwa, N. R. Maarouf, M. H. Darwish, D. W. M. Alhamad, A. Sebastian, M. Hamad, H. A. Omar, G. Orive and T. H. Al-Tel, *Eur. J. Med. Chem.*, 2021, **223**, 113639.
34 K. Strzelecka, U. Piotrowska, M. Sobczak and E. Oledzka, *MDPI*, 2023, preprint, DOI: 10.3390/ijms24021053.
35 F. Bayat, M. Pourmadadi, M. M. Eshaghi, F. Yazdian and H. Rashedi, *J. Cluster Sci.*, 2023, **34**, 2565–2577.
36 M. Rajaei, H. Rashedi, F. Yazdian, M. Navaei-Nigjeh, A. Rahdar and A. M. Díez-Pascual, *J. Drug Deliv. Sci. Technol.*, 2023, **82**, 104307.
37 E. Kahraman, N. Erdol Aydin and G. Nasun-Saygili, *J. Drug Deliv. Sci. Technol.*, 2023, **80**, 104153.
38 Y. Dai, Y. Zhang, T. Ye and Y. Chen, *Molecules*, 2023, **28**(9), 3936.
39 D. N. Heo, D. H. Yang, H. J. Moon, J. B. Lee, M. S. Bae, S. C. Lee, W. J. Lee, I. C. Sun and I. K. Kwon, *Biomaterials*, 2012, **33**, 856–866.
40 M. Das, A. Joshi, R. Devkar, S. Seshadri and S. Thakore, *Bioconjug. Chem.*, 2022, **33**, 369–385.
41 A. Patel and D. Pithadia, *Appl. Catal., A*, 2020, **602**, 117729.
42 D. Dasgupta, M. Das, S. Thakore, A. Patel, S. Kumar and S. Seshadri, *J. Drug Deliv. Sci. Technol.*, 2022, **72**, 103419, DOI: 10.1016/j.jddst.2022.103419.